IEEE Access
Multidisciplinary | Rapid Review | Open Access Journal

Received 25 May 2022, accepted 22 July 2022, date of publication 1 August 2022, date of current version 8 September 2022.

Digital Object Identifier 10.1109/ACCESS.2022.3195499

RESEARCH ARTICLE

An Enhancement and Detection Method for a Glue Dispensing Image Based on the CycleGAN Model

ZHANG XING-WEI[1], ZHANG KE[1], XIE LING-WANG[1,2], ZHAO YONG-JIE[1], AND LU XIN-JIAN[3]

[1]College of Engineering, Shantou University, Shantou 515063, China
[2]Shantou Polytechnic, Shantou 515078, China
[3]Guangdong Goldenwork Robot Technology Ltd., Foshan 528226, China

Corresponding author: Xie Ling-Wang (lwxie1161@stpt.edu.cn)

This work was supported in part by the National Youth Natural Science Foundation of China under Grant 51405279, in part by the Science and Technology Program of Guangdong Province under Grant 2019ST021, in part by the Natural Science Foundation of Guangdong Province of China under Grant 2019A1515011147, and in part by the Special Project for Science and Technology Innovation Team of Foshan City under Grant 2018IT100052.

ABSTRACT During the active alignment focusing process of car camera assembly, lenses and holders need to be gummed by creamy white and translucent UV glue. The quality of glue dispensing can directly influence the performance of car cameras. Because of the translucency of UV glue, the glue dispensing image may present a low contrast situation, which increases the difficulty of vision detection. This paper proposes a method based on CycleGAN to enhance the glue dispensing image and effectively overcome the problems of blurred and low contrast edges. First, the glue part of the image is segmented into twenty regions. Second, the VGG16 model is used to divide the abovementioned twenty regions into high-contrast images and low-contrast images. Next, the CycleGAN model is trained to enhance the low-contrast images, and then convert them to high-contrast images. Finally, glue contours are extracted by using thresholding segmentation and edge detection to ensure that the quality of glue dispensing can be detected. The success rates of the VGG16 model and the CycleGAN model are 96% and 58%, respectively. The results show that the proposed method can effectively enhance the low contrast part of the glue region and improve the detection accuracy. Specifically, it can increase the gray value difference between the glue and the background from 20 to 55, while the background is substantially retained. The detailed information of the edges of the images is enriched. The accuracy of glue edge extraction can be increased to 99%, which is an approximately 75% improvement compared to the methods without enhancement.

INDEX TERMS CycleGAN, detection, glue dispensing, image enhancement.

I. INTRODUCTION

AA (active alignment) focusing is one of the key technologies that affects the imaging quality of a camera in the assembly process of an on-board camera [1]. In the AA focusing process, the relative position between the lens and the front cover with the image sensor is in a completely free state. By adjusting the horizontal position, the vertical position and the tilted angle of the lens relative to the image sensor, the image of the camera can reach the clearest state. Before AA focusing, a circle of UV (Ultraviolet Rays) glue is applied between the front cover and the lens to bond and seal the image sensor. When the amount of glue is large, the glue may drip and contaminate the image sensor. When the amount of glue is small, the adhesion and airtightness are poor, which affects the service life of the camera. Therefore, to ensure the quality of the camera, it is necessary to test the glue quality before AA focusing. However, the key to the testing process is to extract the glue profile completely. Because UV glue is a milky translucent liquid, when the coating layer is thick, the information received by industrial camera imaging is mainly reflected light from the glue. Thus, the contrast

The associate editor coordinating the review of this manuscript and approving it for publication was Yizhang Jiang.

of the sample image is high, and it is easy to extract the glue contour. When the glue is thin, the lens receives the information mostly from the reflected light from the parts at the bottom of the glue. Therefore, the contrast of the sample image is reduced, and it is difficult to extract the glue contour, which seriously affects the accuracy of the detection results and the production efficiency. To solve this problem, it is necessary to systematically study the method of enhancing low-contrast glue images.

Image enhancement is an important factor in the field of image processing. Traditional image enhancement algorithms can be roughly divided into two kinds of processing methods based on the spatial domain and the frequency domain [2], [3]. In the spatial domain, histogram equalization may lose some details due to grayscale merging [4]. Linear enhancement can only be enhanced within a certain gray range of the image, which has great limitations [5], [6]. Nonlinear enhancement, such as Gaussian function transformation, does not significantly enhance the edge information of the image [7]. In the frequency domain, the enhancement algorithm based on directional filter banks has problems, such as reduced image sharpness and it is missing partial features after enhancement [8]. However, the enhancement algorithm based on wavelet transform easily amplifies the noise in the image, which requires further noise reduction [9]. Image enhancement based on neural networks solves the above problems to a certain extent [10]. Lore *et al*. [11] designed an autoencoder based on a deep neural network to enhance the grayscale image, improving the brightness and clarity of the image and proving the feasibility of using deep learning to enhance the image. Xu *et al*. [12] used a conditional generative adversarial network to enhance the super-discrimination-rate reconstructed image. They not only improve the quality of the image reconstruction and enhance the detailed features of edges and textures but also further improve the visual effect. However, the fusion and generation of image features need to be improved continuously. Lal *et al*. [13] proposed a dark light image enhancement algorithm based on a convolutional neural network. Although this method could enhance the overall brightness of the image, it could not only enhance local features without changing other features. Perez *et al*. [14] proposed a kind of underwater image enhancement method that learned from much training by focusing between the degradation of underwater images and the recovery of underwater image models, and then achieved the goal of underwater image enhancement. Wang *et al*. [15] designed an end-to-end image enhancement framework to enhance underwater images, which improved model convergence performance and accuracy, while enhancing the color richness of underwater images. Li and Ma [16] proposed a practical multimodal medical image fusion algorithm based on PCNN and GIF-WSEML in the nonsubsampled contourlet transform domain. Their fusion algorithm had a better performance with improved brightness and contrast of multimodal medical images, and the objective metrics, such as VIFF, QW, API, SD and EN computed by the proposed method also have obvious advantages. However, the fused images of NSCT have lost some details of MRI images, and the results have some noise, which affects the doctor's observation. Guo *et al*. [17] proposed an efficient and effective method to enhance low-light images based on the Retinex-based category. Their low-light image enhancement technique demonstrated that it could feed many vision-based applications, such as edge detection, feature matching, object recognition and tracking, with high visibility inputs, which improved their performance. Iqbal *et al*. [18] used a slide stretching algorithm both on RGB and HIS color models to enhance underwater images. The advantage of applying two stretching models is that they help to equalize the color contrast in the images and solve the lighting problem.

However, the effect of the above image enhancement method often changed the gray value of the whole image, and it was impossible to enhance only the area of interest while the gray value of other areas remained unchanged. Based on the shortcomings of the above image enhancement methods, an improved image enhancement algorithm based on CycleGAN (Cycle Generative Adversarial Networks) for glue-coated images is proposed in this paper. The high- and low-contrast images are first divided by the VGG16 model. Then, the proposed image enhancement algorithm enables low-contrast images to learn the features of high-contrast images to enhance the image region of interest. Finally, the threshold segmentation method is used to extract the glue contour, and then complete glue quality detection.

II. BASIC PRINCIPLES AND METHODS

A. THE CHARACTERISTIC ANALYSIS OF IMAGES AND SAMPLE PRODUCTION OF THE IMAGE OF GLUE

Due to the different thicknesses of glue, the contrast of the edge area of glue in the images are in two different states: high and low, as shown in Figs. 1 and 2. From the perspective of image processing, the higher the contrast between the glue and the background, the easier it is to segment. When the glue is thick, there is a large difference between the gray value of the glue edge area and the background, and the edge contour is clear. It is easy to use image segmentation to directly extract the glue contour, as shown by the red arrow in Fig. 1(b). When the glue thickness is thin, there is a small difference between the gray value of the glue edge area and the background, and the edge contour is fuzzy, as shown by the red arrow in Fig. 2(b). It is difficult to directly segment the image to extract the glue contour. Therefore, it is necessary to enhance the glue-coated image with low contrast. As seen from Fig. 2(a), in a complete image of glue, not all edge areas have low contrast. Some of them may be high, and some of them are low, so the areas with low contrast need to be extracted for enhancement, while the areas with high contrast are reserved. To separate the high- and low-contrast areas in the same glue image, image processing software, Halcon, is used in this paper to divide an image of glue into 20 areas. The processing schematic diagram is shown

in Fig. 3. An image is generated for each area separately. A complete image of the glue can generate 20 sample images, as shown in Fig. 4. Meanwhile, to distinguish the contrast of the sample image, an edge extraction of images is performed using the Otsu threshold segmentation algorithm [19], [20]. The extraction results are shown in Fig. 5. The preliminary determination on the category of the sample image is made by analyzing the roundness and the smoothness of the extracted edges. After that, it is confirmed again by the inspector. The images with glued edges can be accurately extracted by the Otsu threshold segmentation algorithm, which are regarded as the high-contrast sample, while those with the glued edges that cannot be accurately extracted are regarded as low-contrast sample images.

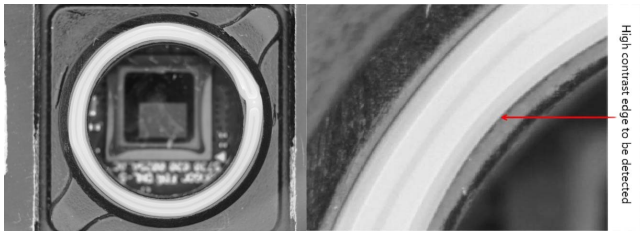

FIGURE 1. High-contrast glue dispensing image; (a) holistic high-contrast coated image; (b) partial high-contrast coated image.

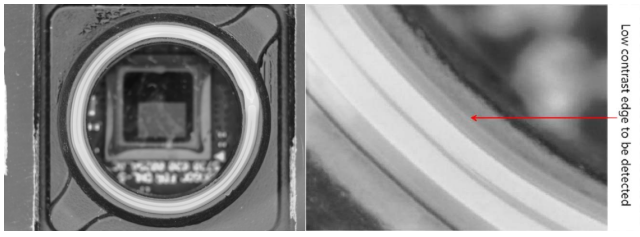

FIGURE 2. Low-contrast glue dispensing image; (a) holistic low-contrast coated image; (b) partial low-contrast coated image.

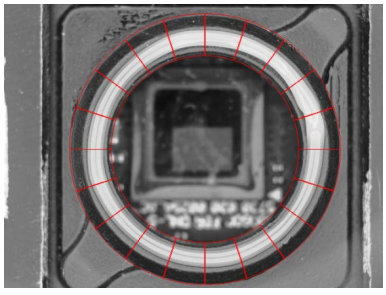

FIGURE 3. Partitioned diagram of the holistic glue dispensing image.

B. VGG16 MODEL

The very deep convolutional network (VGG16) model [21] is a convolutional neural network model proposed by Oxford University in 2014 and won the ILSVRC (ImageNet Large Scale Visual Recognition Challenge) championship in the same year, showing strong classification performance. Due to its practicability and simplicity, it has become one of the most popular convolutional neural network models [22]. Su *et al*. [23] tested the robustness of transfer training for 18 mainstream classification models at present, and the experiment showed that compared with other advanced classification models, the deep stacked VGG16 model could still maintain a higher classification accuracy in transfer training. In industrial applications, it is difficult to obtain enough data samples to finish the training of a complete classification model. Therefore, from the perspective of transferable training, in this paper, we choose the VGG16 model as a classifier to distinguish between high-contrast and low-contrast images of glue.

The structure of the VGG16 model is shown in Fig. 6. The VGG16 model is composed of 13 convolutional layers, 5 pooling layers and 3 fully connected layers. The convolution layer of VGG16 is all stacked up by 3×3 convolution cores, and the convolution layer is raised to the concept of convolution blocks. Each convolution block contains 2-3 convolution layers to ensure that VGG16 has a larger receptive field. Each convolution block is connected by a maximum pooling layer of 2×2, thus reducing the parameters in the neural network and greatly reducing the training difficulty of the network. At the same time, each convolution layer is followed

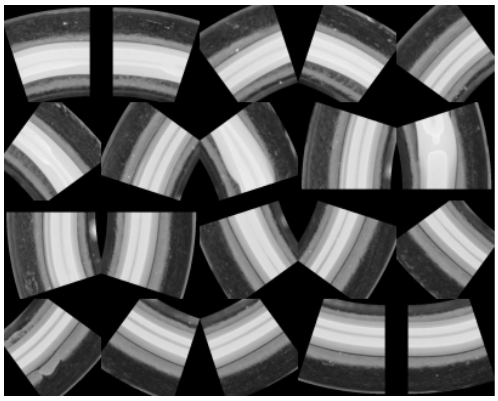

FIGURE 4. Sample graph.

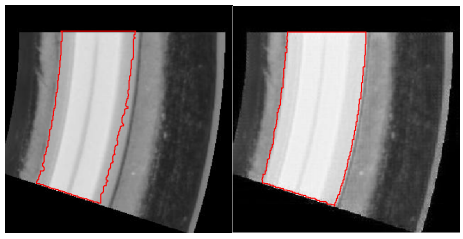

FIGURE 5. Glue edge extraction from glued images; (a) extracted glue edges from low-contrast glue application images; (b) extracted glue edges from high-contrast glue application images.

by a ReLU activation function, whose definition is shown in (1). A large number of activation functions enable VGG16 to have a strong nonlinear transformability, which improves the model's classification performance. The last layer of the VGG16 model uses the softmax function as a classifier to output classification results, whose definition is shown in (2), which reduces the difficulty of training and makes it easier for the network to converge. Moreover, the VGG16 model uses the cross-entropy as the loss function. The definition is shown in the following Formula (3). This cross-entropy function is a convex function, and it facilitates backpropagation to find the global optimal solution. In addition, the calculation process of the numerical instability of the abnormal problem can be solved by using the cross-entropy function together with the softmax function.

$$f(x) = \begin{cases} 0, & x \leq 0 \\ x, & x > 0 \end{cases} \tag{1}$$

$$S_i = \frac{e^i}{\sum_j e^j} \tag{2}$$

$$Loss = -[y \log y' + (1 - y) \log(1 - y')] \tag{3}$$

where y is a true value and y' is the estimate.

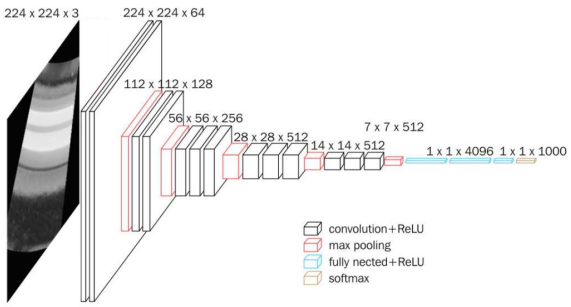

FIGURE 6. Structure diagram of the VGG16 model.

C. SIMPLIFICATION OF THE CYCLEGAN MODEL

CycleGAN is a derivative model of GAN proposed by Zhu *et al*. [24] in 2017. The main contribution of this paper is to propose cyclic consistent loss, which makes the sample image have a one-to-one correspondence with the generated image and solves the problem that many different sample images may produce the same generated image. Engin *et al*. [25] presented an end-to-end network called Cycle-Dehaze for the single image dehazing problem. Their method enhances CycleGAN formulation by combining cycle consistency and perceptual losses to improve the quality of images. However, images may be distorted when scaled. Tmenova *et al*. [26] used CycleGAN to generate vascular images, which solved the problem of insufficient training data in medical images to a certain extent. Chang *et al*. [27] improved the residual structure in the CycleGAN generator to generate calligraphic Chinese characters and achieved good results. At present, CycleGAN is mainly used in style transfer and image generation, but CycleGAN has a wide range of prospects in engineering applications. It is a new attempt to apply CycleGAN in image enhancement and industrial fields in this paper.

In general, the complete CycleGAN model can realize the conversion between the two source domains. In this paper, we only need to convert low-contrast sample images to high-contrast sample images, and we do not need to convert high-contrast sample images to low-contrast images in the reverse process. Therefore, this paper simplifies the model to reduce the redundancy of the model and improve the training speed. The simplified CycleGAN model is shown in Fig. 7. As shown in Fig. 7, the simplified CycleGAN model is composed of two generators and one discriminant, which reduces one discriminant compared with the complete CycleGAN model. Its working principle is as follows:

(1) First, the low-contrast images in the sample set of the source domain are generated by generator G to generate high-contrast images.

(2) Another generator, F, is used to regenerate the low-contrast image, and the source domain information is recovered by comparing the similarity between the original low-contrast image and the generated low-contrast image, i.e., calculating the cyclic consensus loss, as shown in the dotted circle in Fig. 6.

(3) Finally, discriminant D is used to distinguish the generated high-contrast images from the high-contrast images in the sample set.

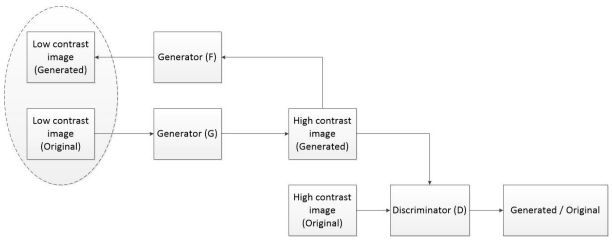

FIGURE 7. Structure diagram of the CycleGAN model.

The loss functions of generator G and discriminator D are defined in (4) and (5). A discriminant loss increases with a decreasing generator loss. Similarly, the generator loss increases with a decreasing discriminator loss. The generator and discriminator in the simplified CycleGAN model are also against each other in the training process to improve the performance of their respective networks.

$$L_{gen}(G, D, X) = E_{x \sim pdata(x)}[(D(G(x)) - 1)^2] \tag{4}$$

$$L_{dis}(G, D, X, Y) = E_{y \sim pdata(y)}[(D(y) - 1)^2] + E_{x \sim pdata(x)}[D(G(x))^2] \tag{5}$$

The loss function definition of the entire simplified CycleGAN model is shown in (6), where the third item on the right side of the equal sign is the cyclic consistent loss.

$$L(G, F, D_Y) = L_{gen}(G, D, X) + L_{dis}(G, D, X, Y) + \lambda L_{cyc}(G, F) \tag{6}$$

$$L_{cyc}(G,F) = E_{x\sim p_{data}(x)}\left[\|F(G(x)) - x\|_1\right] + E_{y\sim p_{data}(y)}\left[\|F(G(y)) - y\|_1\right] \quad (7)$$

1) IMPROVEMENT OF CYCLIC CONSISTENT LOSS

As seen in (7), the original CycleGAN model uses the MEA loss function for the cyclic consistent loss. Although the MEA [28] loss function is more robust to outliers, the gradient of the MEA loss function is always the same when the neural network parameters are updated, resulting in a large gradient even for a small loss value. This makes it difficult for the neural network to converge. Although the gradient of the MSE [28] loss function changes with the change in the loss, it has a large gradient when the loss is large. Additionally, the gradient decreases correspondingly when the loss tends to be 0, but the MSE loss function is more sensitive to outliers. Therefore, the logarithmic hyperbolic cosine function is selected as the cyclic consistent loss function of the simplified CycleGAN model in this paper, and its function expression is shown in (8).

$$y = \log(\cosh(x)) \quad (8)$$

Log-Cosh [29], MAE and MSE loss functions are shown in Fig. 8. As seen in Fig. 8, when the loss value is large, Log-Cosh is close to $abs\,(x) - \log(2)$, which indicates that Log-Cosh has the advantage of the MAE loss function being relatively robust to outliers. When the loss is small, Log-Cosh is close to $x^2/2$, which indicates that Log-Cosh also has the advantage that the MSE loss function can change the gradient according to the loss to ensure that the neural network can converge faster. The improved cyclic uniform loss is defined in (9), where A is the hyperparameter, which is used to control the proportion of cycle uniform loss in the total loss. It could be seen from Figs. 9, 10 and 11 that Log-Cosh loss function makes the loss of generator and discriminator more stable during the training of neural network.

$$L_{cyc}\,(G,F) = \lambda \times E_{x\sim pdata(x)}\left[\log(\cosh(F(G(x)) - x))\right] \quad (9)$$

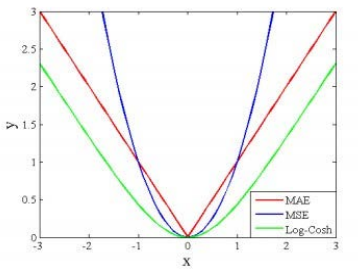

FIGURE 8. Different loss function graphs.

2) CYCLEGAN'S GENERATOR

Generators F and G are important components of the CycleGAN network model, and their structure is shown in Fig. 12.

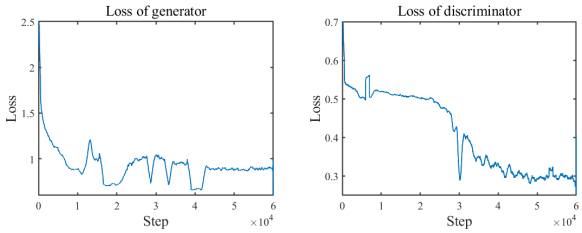

FIGURE 9. Different losses from MAE; (a) generator loss function image; (b) discriminator loss function image.

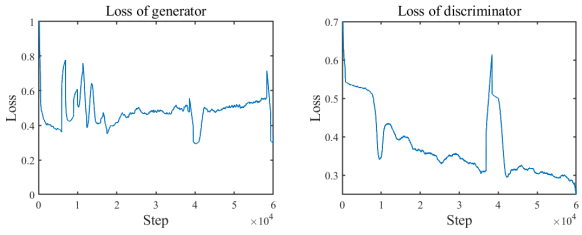

FIGURE 10. Different losses from MSE; (a) generator loss function image; (b) discriminator loss function image.

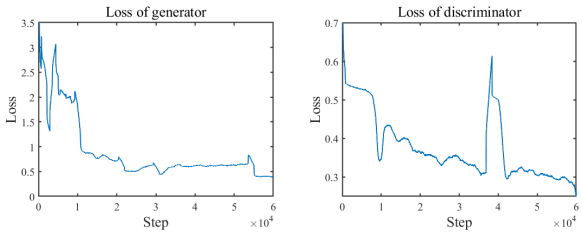

FIGURE 11. Different losses from Log-Cosh; (a) generator loss function image; (b) discriminator loss function image.

F and G are used to generate low-contrast and high-contrast images, respectively. The generator is mainly composed of three convolution layers, nine residual layers, two deconvolution layers and a final convolution layer. The structure of the residual layer is shown in Fig. 13. Following each convolution layer and deconvolution layer, instance normalization is used to speed up the convergence of the model and prevent gradient explosions. The generator uses the ReLU activation function to improve the nonlinear transformability. Two convolutional layers are used in each residual layer to extract features and combine them with the original image features to prevent the loss of image information due to the increase in the number of convolutional layers and better retain the basic features of the original image, such as the edge and background in the low contrast image. The generator uses two deconvolution layers to restore the low-level features of the image and adds the features of the target image to the original image, such as the gray value of the glue in the high contrast image to achieve the enhanced contrast

effect. Finally, one convolution layer is used to complete the generation of high-contrast images.

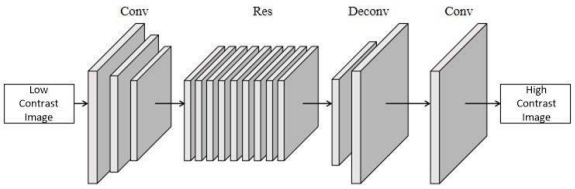

FIGURE 12. Structural diagram of the generator.

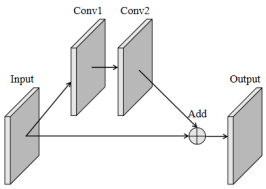

FIGURE 13. Structural diagram of the ResNet block.

3) CYCLEGAN'S DISCRIMINATOR

In the CycleGAN model, the discriminator plays an important role in confrontation training. It can be seen from (4) and (5) that in addition to the loss of the discriminator itself, the loss of the generator is also directly related to the discriminator. Therefore, the performance of the discriminator directly determines the training results of the whole CycleGAN model. The structure of CycleGAN's discriminator is shown in Fig. 14. The function of the discriminator is to identify whether the image is the original high-contrast image or the high-contrast image generated by the generator. The discriminator mainly consists of five convolutional layers, and the second to fourth layers also adopt instance normalization. The activation function of the discriminator uses the LeakyReLU function, as defined in (10). LeakyReLU resolves the gradient disappearance problem that might exist in the ReLU function and improves the stability of the discriminator during training. The last convolution layer uses the sigmoid function to classify the output results, and its definition is shown in (11). When the identification is the original high-contrast image, the output of the last convolution layer is 1. When the determination is an image generated by the generator, the output of the last convolution layer is 0.

$$f(x) = \begin{cases} \alpha x, & x \leq 0 \\ x, & x > 0 \end{cases} \tag{10}$$

$$S(x) = \frac{1}{1 + e^{-x}} \tag{11}$$

D. SAMPLE DATA EXPANSION METHOD

Because the amount of sample data obtained in industrial applications is limited and less sample data leads to underfitting of the neural network, it is necessary to enlarge the sample image. Halcon is used to divide one complete image of glue into twenty sample images. Then, for each sample image, the method of rotation and mirroring is adopted to expand the sample data. The specific methods are as follows:

(1) Rotate the image by 90°, 180° and 270°, and the sample data can be expanded 3 times after this step.

(2) Mirror the images according to the first quadrant, second quadrant and third quadrant. After this step, the sample data can be expanded by 3 times.

(3) Mirror the 90° image according to the second quadrant. After this step, the sample data can be expanded by 1 time. Through the above method, the sample data can be expanded by 7 times.

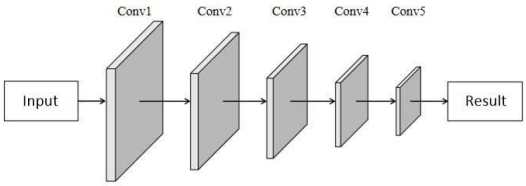

FIGURE 14. Structural diagram of the discriminator.

III. THE RESULTS AND DISCUSSION

Computers with hardware configurations, such as CPU-Intel Xeon W3175-X and GPU-NVIDIA Quadro RTX6000 24G are used in this study. Both the VGG16 model and the CycleGAN model are implemented programmatically on TensorFlow, which is an open-source deep learning framework.

A. VGG16 MODEL CLASSIFICATION

When training the VGG16 model, the gradient descent method is used to solve the optimization method, the batch size is 64, and the learning rate is 0.0001. The pretraining model is used to freeze the weight of neural network nodes in the first 13 convolutional layers of VGG16, and its own sample set is used to train the last 3 fully connected layers.

A total of 2000 sample data were used to train the VGG16 model, including 1000 high-contrast images and 1000 low-contrast images. Fifty high-contrast images and 50 low-contrast images without sample expansion are used as the test set to test the classification and generalizability of the model. Since the VGG16 model has more than 100 million parameters that need to be trained, if all sample data are used for training, network training will take a long time. Therefore, the pretraining model is used in this paper for transfer learning, and the number of layers with pretraining weights and the detection accuracy in the training set are shown in Table 1. It can be seen that, for the current sample size, the classification accuracy of the first 13 layers using pretrained weights is the highest. Therefore, the parameters of the first 13 convolutional layers are used in this paper with pretrained weights.

In the training process, the loss of the model and the accuracy of detection are shown in Figs. 15 and 16. It can be

TABLE 1. Detection accuracy of different pretraining weight layers.

Pretraining weight layers	Test set accuracy
11	51%
12	63%
13	96%
14	87%
15	71%

seen that with the increase in the number of training steps, the loss of the model decreases and the accuracy rate increases. Finally, during the training process, the loss of the model is close to 0, while the accuracy rate is close to 100%. Through experiments, the accuracy rate of the model after training on the test set also reaches 96%, indicating that the model does not fit during training, and the generalization performance of the model is good. The classification results of the VGG16 model after the training are shown in Fig. 17. It can be seen that the classification results have high accuracy. In conclusion, the model has good classification performance after training and can effectively distinguish high-contrast images from low-contrast images.

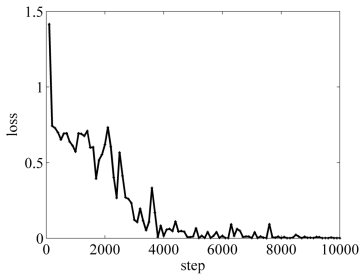

FIGURE 15. Curve of loss.

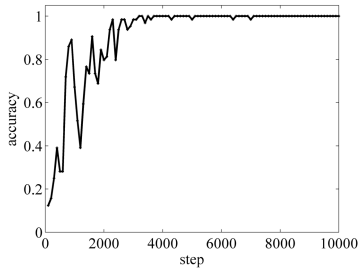

FIGURE 16. Curve of accuracy.

B. CYCLEGAN MODEL IMAGE ENHANCEMENT

When the CycleGAN model is trained, the Adam [30] solver is used with a batch size of 1. All networks are trained from scratch with a learning rate of 0.0002. On the activation function of the discriminator, α in (10) is 0.2. In this paper, 3600 sample data are used to train the CycleGAN model, including 1800 high-contrast images and 1800 low-contrast

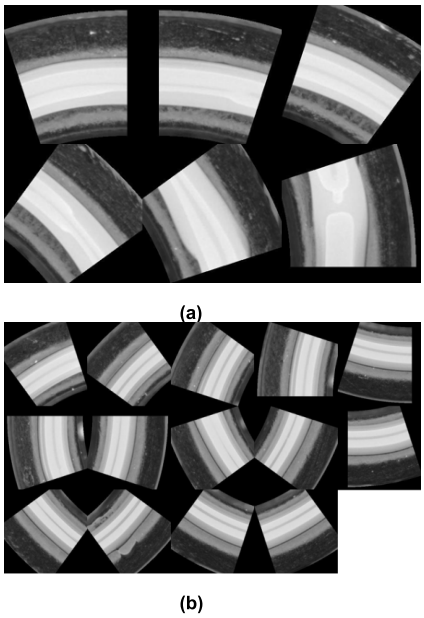

FIGURE 17. Classification result of the VGG16 model; (a) high-contrast image; and (b) low-contrast image.

images. Fifty low-contrast images without sample expansion are used as the test set to test the enhancement effect and the generalizability of the model. As shown in (6), the hyperparameter λ determines the proportion of the cyclic uniform loss in the whole model loss. The enhanced image results for different λ values are shown in Fig. 18. When λ =2, the enhanced image is rough, and the edge is fuzzy. When λ =6, the contrast improved obviously, and the edge appears blurry. When λ =18 and 22, the enhanced image changes the edge contour of the original image, which affects the next detection. When λ =10 and 14, the enhancement effect is good, but when λ =10, the background gray value is closer to the original image. Therefore, we set λ =10 in (6).

In the training process, discriminant loss, generator loss and cycle consistent loss are shown in Fig. 19. Fig. 19(a) shows that the discriminator and the generator are trained separately at the beginning and maintain the initial equilibrium state. Since the structure of the discriminant is simpler than that of the generator so that fewer parameters need to be trained, the discriminant trains faster and has a better discriminant function in the first place. As a result, the loss of the discriminant decreases while the loss of the generator increases, and then the whole model enters the phase of adversarial training. After a long training, the generator training is completed, and the whole model forms a relatively balanced state again. At this time, both the generator and the discriminator have good performance. Fig. 19(b) shows that the cyclic consensus loss decreases continuously as the number of training steps increases, which means that the generated image has a high similarity to the original image and that the generator also has good performance.

In the test set, the CycleGAN model has a success rate of 58% for substantial enhancement of low-contrast images.

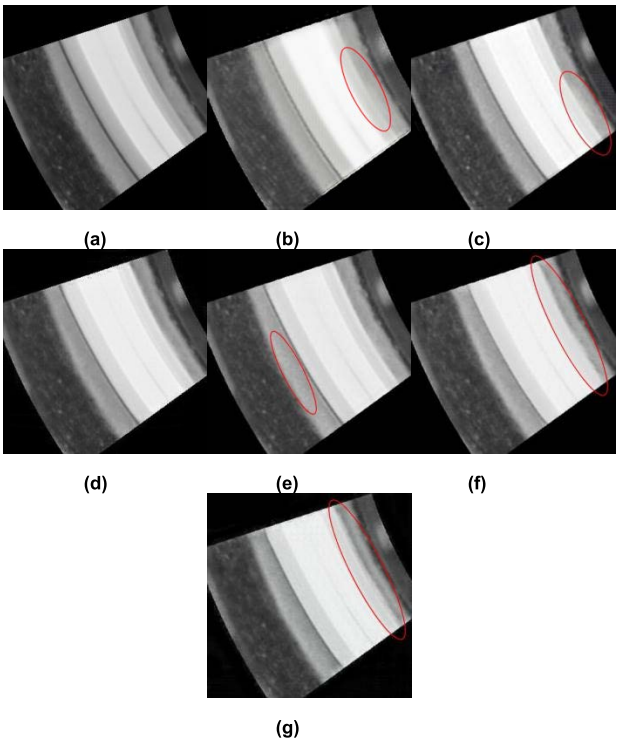

FIGURE 18. Image generation of different λ values: (a) original low contrast glue dispensing image; (b) enhanced image when λ =2; (c) enhanced image when λ =6; (d) enhanced image when λ =10; (e) enhanced image when λ =14; (f) enhanced image when λ =18; (g) enhanced image when λ =22.

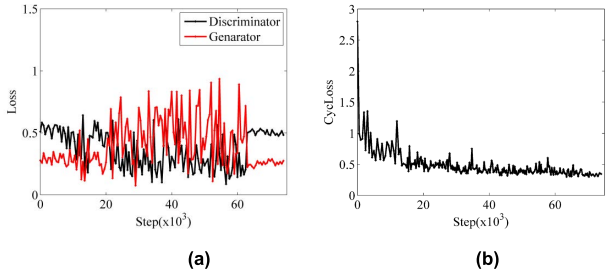

FIGURE 19. Loss of CycleGAN model; (a) loss of generator and discriminator; (b) loss of cycle consistency.

Some of the enhancements to the test set are shown in Fig. 20. After the enhancement by the CycleGAN model, it can be clearly seen that the gray value of the whole glue becomes higher, especially the gray value of the edge area of the glue, which increases considerably, while the gray value of the background part remains unchanged. Thus, the contrast between the glue and the background is overall improved. The gray value difference between the edge area of the original low-contrast image glue and the background area is only approximately 20, but after enhancement, the gray value difference reaches approximately 55, which greatly reduces the difficulty of the following threshold segmentation. The enhancement effect of a complete glue-coating image is shown in Fig. 21(a). In Fig. 21(a), the area inside the blue circle indicates that the VGG16 model discriminates it as a high-contrast image, so it does not need to be enhanced. The area inside the red circle is identified as a low-contrast image by the VGG16 model. After enhancement, the contrast of the edge area can be considerably improved. As shown in Fig. 21(b), the 20 local sample images still maintain good integrity and continuity after being enhanced and stitched back together, and the gray values of the glue and the background between each locally enhanced image maintain good consistency, which is convenient for the following threshold segmentation and edge extraction operations.

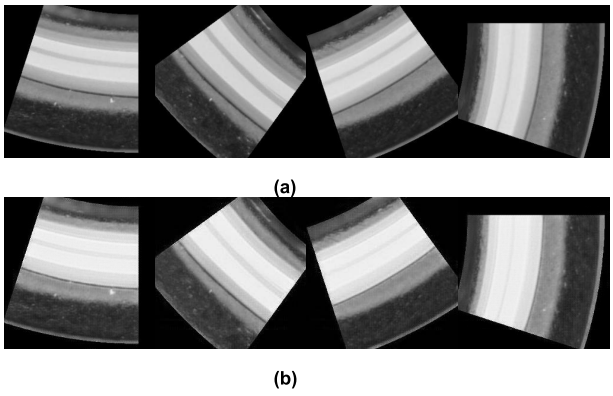

FIGURE 20. Samples of enhancement results in the test data; (a) test images; (b) images of enhancement results.

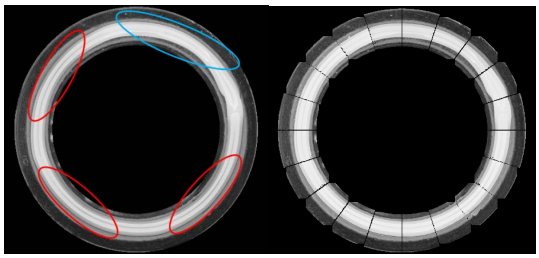

FIGURE 21. Comparison of the original image and the overall enhancement image; (a) original glue dispensing image; (b) holistic enhanced image.

To further evaluate the enhancement performance of the proposed method in this paper, two other image enhancement algorithms proposed by Iqbal Guo *et al*. [17] and *et al*. [18] are also tested on this glue dispensing image dataset. It is shown that the computational processing speeds of the three algorithms are not much different. The image enhancement results are shown in Fig. 22. The image displayed in Fig. 22(d) is the result of dataset processing using the underwater dark light enhancement algorithm proposed by Guo *et al*. [17]. Fig. 22(e) is the result of processing the dataset using the dark light background enhancement algorithm proposed by Iqbal *et al*. [18]. It can be directly noted

that the proposed method provides a better enhancement effect of the interest region of the glue dispensing image. Although the underwater enhancement algorithm and the dark light enhancement algorithm play a certain role in enhancing the glued image, these two algorithms cannot enhance the area of interest while keeping the gray value of other areas unchanged. For a more quantitative representation of the effect of the different algorithms, histograms of the grayscale intensity of the images of Fig. 22 are shown in Fig. 23. The results show that the grayscale histogram of the proposed method in this paper is the most similar to the histogram distribution of the high-contrast glue images between the three enhancement algorithms. Furthermore, an increase in the number of high brightness pixels in the image suggests that the glue image is enhanced. There is an obvious increase in the high brightness pixels in the interest area when the low-contrast image is enhanced by our cycleGAN algorithm. The other two algorithms do not provide the same enhancement effect in the interest area of the low-contrast image.

C. GLUE CONTOUR EXTRACTION AND DETECTION

Before the low-contrast image of glue is enhanced, the method of combining fixed threshold segmentation and Otsu threshold segmentation commonly used in the industry is used to extract the glue contour. As shown in Fig. 24(a), the extracted glue has a rough edge and a larger contour error. Systematic experimental results show that the success rate of accurately extracting the low-contrast glue profile is only 24% in this condition, which is far from meeting the requirements of product qualification rate control. However, the image of glue with a low contrast region is enhanced by our proposed algorithm. Because of the high contrast, the glue contour can be extracted directly with fixed threshold segmentation after the enhancement. As shown in Fig. 24(b), it can be seen that the glue contour is accurately extracted, and the edge is smoother than that without enhancement. The stability and the accuracy of glue quality detection is improved.

The overall coated edge extraction of the glue coating is also performed in the Gluing process test platform, as shown in Fig. 25. We test three enhancement methods. The results of edge extraction are listed in Fig. 26. In Fig. 26(b), it can be seen that the part of the glue contour edge required for detection is considerably enhanced. The success rate of accurately extracting low-contrast glue contours is increased to approximately 99% by our method, which can meet the basic requirements of engineering tests. In addition, the results of the dark light enhancement algorithm and the underwater image enhancement algorithm for glued edge extraction can also enhance the overall details of the glue-coated image, as shown in Fig. 26(c) and (d). After extracting the gluing edge of the enhanced images with fixed threshold segmentation, it was found that the success rate of extracting low-contrast glue contour parts is also increased. However, after manual inspection of the inspector, we found that the shape accuracy of

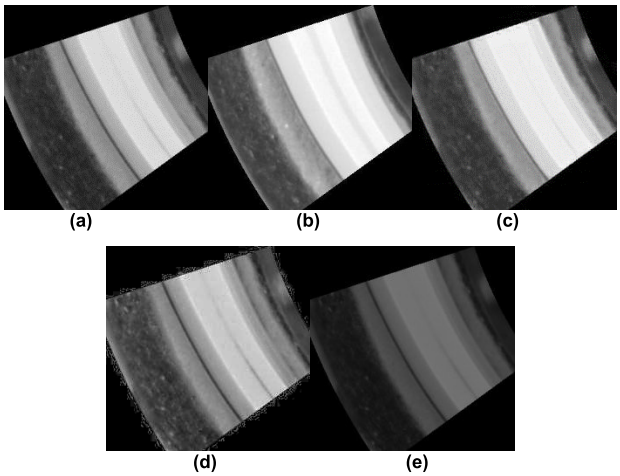

FIGURE 22. Results of other enhancement algorithms; (a) low contrast glue image; (b) high contrast glue image; (c) the image after enhancement by the cycleGAN algorithm; (d) the image enhanced by using the underwater enhancement algorithm proposed by Guo *et al.* [17] (e) the image enhanced by using the dark light background enhancement algorithm proposed by Iqbal *et al.* [18].

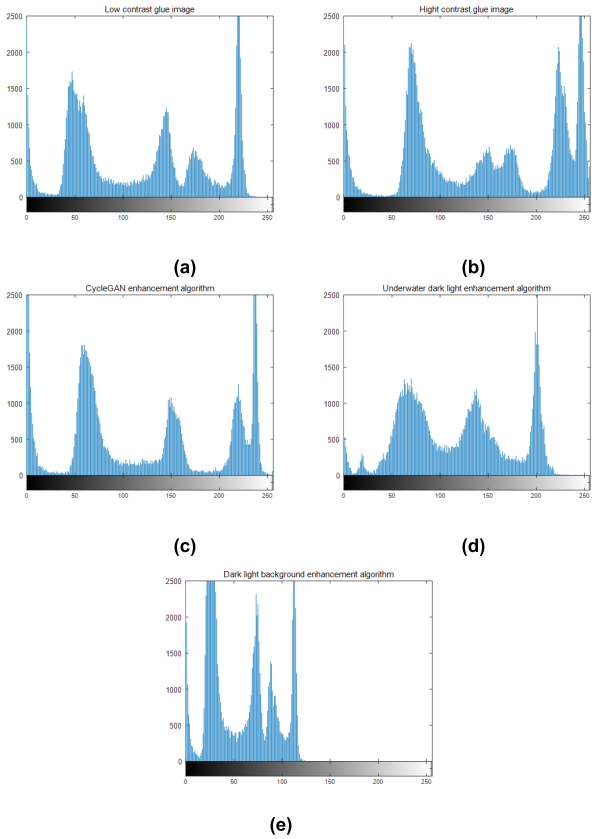

FIGURE 23. Grayscale histogram of Fig. 21; (a) is the grayscale histogram of Fig. 21(a); (b) is the grayscale histogram of Fig. 21(b); (c) is the grayscale histogram of Fig. 21(c); (d) is the grayscale histogram of Fig. 21(d); (e) is the grayscale histogram of Fig. 21(e).

the extracted contour after sample enhancement is still quite different from the actual gluing contour edge (e.g., as marked

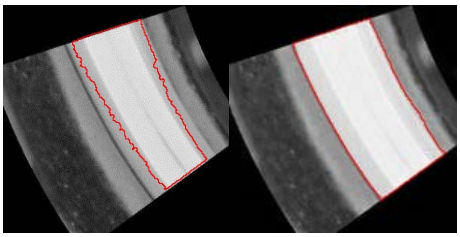

(a) (b)

FIGURE 24. Glue edge extraction before and after enhancement; (a) edge extraction results before enhancement; (b) edge extraction results after enhancement.

in Fig. 26(c) and (d)), which means that the success rate of the sizing inspection cannot be improved and may have a substantial impact on the accuracy of the subsequent AA focusing process.

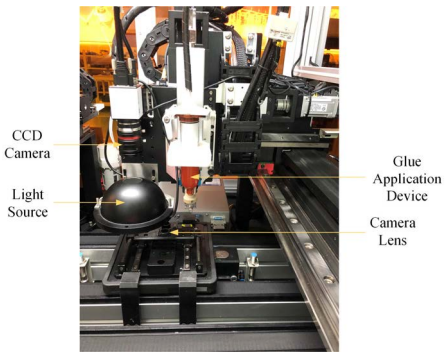

FIGURE 25. Comparison of the original image and the overall image.

After performing threshold segmentation and expansion and corrosion morphological operations on the samples shown in Fig. 21(b), the glue area of the images of glue can be obtained, as shown in Fig. 27. It can also be seen in Fig. 26(b) that a complete glue contour can be obtained by edge extraction of the obtained glue area. After obtaining the glue contour, the quality of the glue can be determined according to the characteristics of the contour. There are three main criteria for determining the quality of the glue: (1) the uniformity criterion: according to the obtained glue contour, the maximum glue width and the minimum glue width can be calculated to determine the uniformity of the glue; (2) the adhesive width criterion: determination of whether the adhesive width of the glue meets the requirements by calculating the radius difference between the inner and outer contour fitting circles of glue, as shown in Fig. 28; (3) the offset criterion: the distance between the average value of the fitting center of the inner and outer contour of the glue and the center of the reference circle of the parts is calculated to determine whether the glue is biased, as shown in Fig. 29. The green circle is the reference circle of the part, and the green point is the center of the reference circle. The red circle is the fitting circle of the inner and outer contours, and the red dot is the

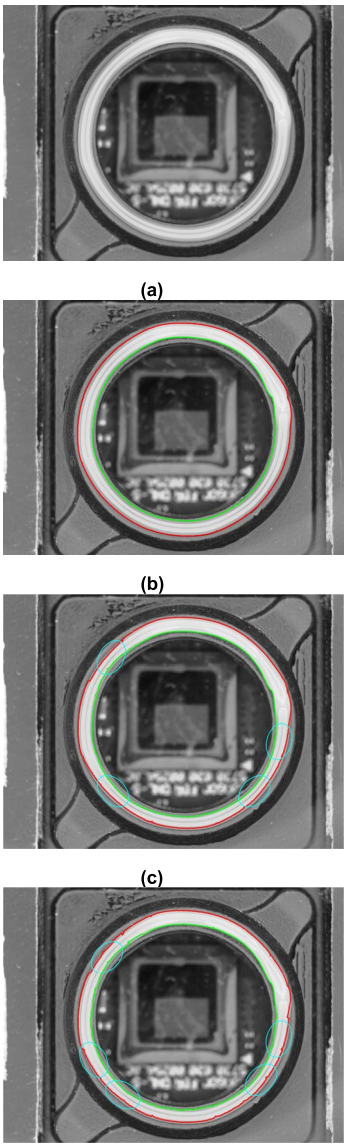

(a) (b) (c) (d)

FIGURE 26. Glue edge extraction result image; (a) Original low-contrast glue dispensing image; (b) Glue edge extraction of glued images after enhancement by the CycleGAN enhancement algorithm; (c) Glue edge extraction of glued images after enhancement by using the underwater enhancement algorithm; (d) Glue edge extraction of glued images after enhancement by using the dark light background enhancement algorithm.

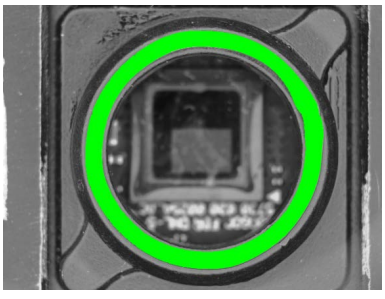

FIGURE 27. Region of glue.

average value of the center of the fitting circle. The final test result is shown in Fig. 30.

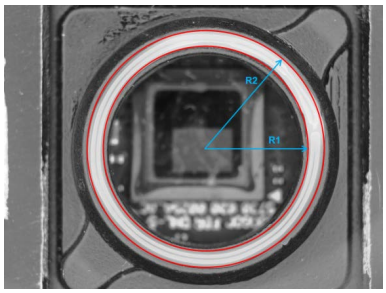

FIGURE 28. Diagram of the glue width criterion.

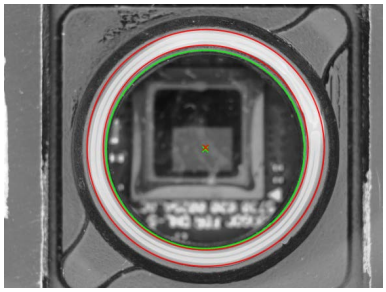

FIGURE 29. Diagram of the eccentricity criterion.

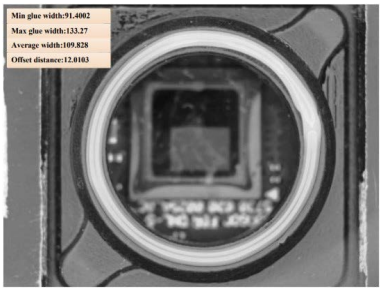

FIGURE 30. Image of the detection result.

IV. CONCONCLUSION

To solve the problems of low glue contrast and the difficulty to detect the images of glue in the process before AA focusing of the vehicle-mounted camera assembly, this paper proposes a method based on CycleGAN to enhance the images of glue of the camera samples to improve the detection accuracy of the glue quality. The VGG16 model is used to identify areas with low contrast. The CycleGAN model is used to enhance the low-contrast image, and finally, the quality of the glue is tested. The results show that the classification success rate of the VGG16 model in the test set reaches 96%, and it can effectively distinguish the low-contrast and the high-contrast images of glue. The CycleGAN model can substantially improve the gray value of the low-contrast glue area in the images of glue. In the condition of maintaining the original gray value of the background area, the difference in the gray value between the glue and the background is increased from approximately 20 to 55, which improves the contrast of the images of the glue and reduces the difficulty of detection. In the test set, the enhancement success rate is 58%. For the enhanced low-contrast image of glue, the accuracy of extracting the glue contour reaches 99%, which is a 75% improvement over the unenhanced image. At present, the research of this paper mainly relies on the data expansion method to increase the sample data. With the increase in the original sample size, the success rate of the enhanced image is also improved. Therefore, it is considered that this method has wide application prospects in automatic industrial manufacturing. However, the success rate of the enhanced image of the CycleGAN model in the current method cannot fully meet the absolute accuracy requirements of product detection on the actual industrial automated assembly production line. At the same time, in the actual industrial application environment, usually, considerable manpower and material resources are needed to obtain enough data samples. Therefore, in our future studies, further research will be conducted on improving the performance of the CycleGAN model in the case of a low sample data size.

ACKNOWLEDGMENT

The authors are gratefully acknowledged the financial support. They would also like to thank the anonymous reviewers for their very useful comments.

REFERENCES

[1] K. Bitzer and A. By, "Active alignment for cameras in mobile devices and automotive applications," in *Proc. 12th Electron. Packag. Technol. Conf.*, Singapore, Dec. 2010, pp. 260–264.
[2] G. Singh and A. Mittal, "Various image enhancement techniques—A critical review," *Int. J. Innov. Sci. Res.*, vol. 10, no. 2, pp. 267–274, Oct. 2014.
[3] Y. Qi, Z. Yang, W. Sun, M. Lou, J. Lian, W. Zhao, X. Deng, and Y. Ma, "A comprehensive overview of image enhancement techniques," *Arch. Comput. Methods Eng.*, vol. 29, no. 1, pp. 583–607, Jan. 2022, doi: 10.1007/s11831-021-09587-6.
[4] S. Yang, J. H. Oh, and Y. Park, "Contrast enhancement using histogram equalization with bin underflow and bin overflow," in *Proc. Int. Conf. Image Process.*, Barcelona, Spain, Sep. 2003, p. 881.
[5] V. Sharma, J. Y. Hardeberg, and S. George, "RGB-NIR image enhancement by fusing bilateral and weighted least squares filters," *J. Imag. Sci. Technol.*, vol. 61, no. 4, p. 40409, Jul. 2017, doi: 10.2352/J.ImagingSci.Technol.2017.61.4.040409.
[6] E. Zhao and J. Gao, "An adaptive low-illumination image enhancement algorithm based on weighted least squares optimization," *J. Phys., Conf.*, vol. 2181, no. 1, Jan. 2022, Art. no. 012011, doi: 10.1088/1742-6596/2181/1/012011.
[7] W. Zhao, Z. Xu, J. Zhao, F. Zhao, and X. Han, "Infrared image detail enhancement based on the gradient field specification," *Appl. Opt.*, vol. 53, no. 19, pp. 4141–4149, Jul. 2014, doi: 10.1364/AO.53.004141.
[8] M. A. U. Khan and T. M. Khan, "Fingerprint image enhancement using data driven directional filter bank," *Optik*, vol. 124, no. 23, pp. 6063–6068, Dec. 2013, doi: 10.1016/j.ijleo.2013.04.071.
[9] D. Heric and B. Potocnik, "Image enhancement by using directional wavelet transform," in *Proc. 28th Int. Conf. Inf. Technol. Interfaces*, Cavtat, Croatia, 2006, pp. 201–206.
[10] D. Perdios, M. Vonlanthen, A. Besson, F. Martinez, M. Arditi, and J.-P. Thiran, "Deep convolutional neural network for ultrasound image enhancement," in *Proc. IEEE Int. Ultrason. Symp. (IUS)*, Kobe, Japan, Oct. 2018, pp. 1–4.
[11] K. G. Lore, A. Akintayo, and S. Sarkar, "LLNet: A deep autoencoder approach to natural low-light image enhancement," *Pattern Recognit.*, vol. 61, pp. 650–662, Jan. 2017, doi: 10.1016/j.patcog.2016.06.008.
[12] C. Xu, Y. Cui, Y. Zhang, P. Gao, and J. Xu, "Image enhancement algorithm based on generative adversarial network in combination of improved game adversarial loss mechanism," *Multimedia Tools Appl.*, vol. 79, nos. 13–14, pp. 9435–9450, Apr. 2020, doi: 10.1007/s11042-019-07776-x.

[13] K. J. Lal, D. Rana, and A. S. Parihar, "A comparative study on CNN based low-light image enhancement," in *Proc. 11th Int. Conf. Cloud Comput., Data Sci. Eng. (Confluence)*, Noida, India, Jan. 2021, pp. 459–464.
[14] J. Perez, A. C. Attanasio, N. Nechyporenko, and P. J. Sanz, "A deep learning approach for underwater image enhancement," in *Biomedical Applications Based on Natural and Artificial Computing*. Almería, Spain: Springer, 2017, pp. 183–192.
[15] Y. Wang, J. Zhang, Y. Cao, and Z. Wang, "A deep CNN method for underwater image enhancement," in *Proc. IEEE Int. Conf. Image Process. (ICIP)*, Beijing, China, Sep. 2017, pp. 1382–1386.
[16] L. Li and H. Ma, "Pulse coupled neural network-based multimodal medical image fusion via guided filtering and WSEML in NSCT domain," *Entropy*, vol. 23, no. 5, p. 591, May 2021, doi: 10.3390/e23050591.
[17] X. Guo, Y. Li, and H. Ling, "LIME: Low-light image enhancement via illumination map estimation," *IEEE Trans. Image Process.*, vol. 26, no. 2, pp. 982–993, Dec. 2017, doi: 10.1109/TIP.2016.2639450.
[18] K. Iqbal, R. A. Salam, A. Osman, and A. Z. Talib, "Underwater image enhancement using an integrated colour model," *IAENG Int. J. Comput. Sci.*, vol. 34, no. 2, pp. 1–6, Dec. 2007.
[19] X.-C. Yuan, L.-S. Wu, and Q. Peng, "An improved Otsu method using the weighted object variance for defect detection," *Appl. Surf. Sci.*, vol. 349, pp. 472–484, Sep. 2015, doi: 10.1016/j.apsusc.2015.05.033.
[20] T. Y. Goh, S. N. Basah, H. Yazid, M. J. A. Safar, and F. S. A. Saad, "Performance analysis of image thresholding: Otsu technique," *Measurement*, vol. 114, pp. 298–307, Jan. 2018, doi: 10.1016/j.measurement.2017.09.052.
[21] K. Simonyan and A. Zisserman, "Very deep convolutional networks for large-scale image recognition," 2014, *arXiv:1409.1556*.
[22] M. Mahdianpari, B. Salehi, M. Rezaee, F. Mohammadimanesh, and Y. Zhang, "Very deep convolutional neural networks for complex land cover mapping using multispectral remote sensing imagery," *Remote Sens.*, vol. 10, no. 7, p. 1119, Jul. 2018, doi: 10.3390/rs10071119.
[23] D. Su, H. Zhang, H. Chen, J. Yi, P.-Y. Chen, and Y. Gao, "Is robustness the cost of accuracy? A comprehensive study on the robustness of 18 deep image classification models," in *Computer Vision*. Munich, Germany: Springer, 2018, pp. 644–661.
[24] J.-Y. Zhu, T. Park, P. Isola, and A. A. Efros, "Unpaired Image-to-Image translation using cycle-consistent adversarial networks," in *Proc. IEEE Int. Conf. Comput. Vis. (ICCV)*, Venice, Italy, Oct. 2017, pp. 2242–2251.
[25] D. Engin, A. Genc, and H. K. Ekenel, "Cycle-dehaze: Enhanced CycleGAN for single image dehazing," in *Proc. IEEE/CVF Conf. Comput. Vis. Pattern Recognit. Workshops (CVPRW)*, Salt Lake City, UT, USA, Jun. 2018, pp. 938–9388.
[26] O. Tmenova, R. Martin, and L. Duong, "CycleGAN for style transfer in X-ray angiography," *Int. J. Comput. Assist. Radiol. Surg.*, vol. 14, no. 10, pp. 1785–1794, Oct. 2019, doi: 10.1007/s11548-019-02022-z.
[27] B. Chang, Q. Zhang, S. Pan, and L. Meng, "Generating handwritten Chinese characters using CycleGAN," in *Proc. IEEE Winter Conf. Appl. Comput. Vis. (WACV)*, Lake Tahoe, NV, USA, Mar. 2018, pp. 199–207.
[28] A. Lahoulou, A. Bouridane, E. Viennet, and M. Haddadi, "Full-reference image quality metrics performance evaluation over image quality databases," *Arabian J. Sci. Eng.*, vol. 38, no. 9, pp. 2327–2356, Sep. 2013, doi: 10.1007/s13369-012-0509-6.
[29] X. Xu, J. Li, Y. Yang, and F. Shen, "Toward effective intrusion detection using log-cosh conditional variational autoencoder," *IEEE Internet Things J.*, vol. 8, no. 8, pp. 6187–6196, Apr. 2021, doi: 10.1109/JIOT.2020.3034621.
[30] D. P. Kingma and J. Ba, "Adam: A method for stochastic optimization," 2014, *arXiv:1412.6980*.

ZHANG XING-WEI received the B.E. degree in thermal energy and power engineering, the M.E. degree in mechanical and electronic engineering, and the Ph.D. degree in fluid machinery and engineering from the Harbin Institute of Technology, Harbin, China, in 2003, 2006, and 2011, respectively. He is currently an Associate Professor with the Department of Mechatronics Engineering, Shantou University. He is mainly engaged in the design of special bionic robots, design and analysis of bionic mechanical structures, flow control, machine vision, and image processing research direction.

ZHANG KE received the B.E. degree in mechanical engineering from Ningbo University, Ningbo, China, in 2020. He is currently pursuing the master's degree in mechanical engineering with Shantou University. His current research interests include fluid dynamics data visualization, computer vision, and image generation.

XIE LING-WANG received the B.E. and M.E. degrees in mechanical engineering from Shantou University, Shantou, China, in 2017 and 2020, respectively. Since 2020, he has been working with the Department of Mechanical and Electrical Engineering, Shantou Polytechnic. His current research interests include image processing, deep learning, and image enhancement.

ZHAO YONG-JIE received the B.E. degree in metallurgy engineering from Northeastern University, Shenyang, China, in 2000, the M.E. degree in mechanical engineering from the Tianjin University of Technology, Tianjin, China, in 2003, and the Ph.D. degree in mechanical engineering from Tianjin University, Tianjin, in 2006. From 2006 to 2008, he has worked as a Postdoctoral Research Fellow at the State Key Laboratory of Mechanical System and Vibration, Shanghai Jiao Tong University, Shanghai, China. He is currently a Professor with the Department of Mechatronics Engineering, Shantou University, China. His current research interests include kinematics, dynamics, performance evaluation and control, and multidisciplinary optimization design of manipulators.

LU XIN-JIAN received the B.E. degree in aerospace welding engineering from the Nanchang Institute of Aeronautical Technology, in 1983. He is currently the General Manager of Guangdong Goldenwork Robot Technology Ltd. He is a part-time Professor with Nanchang Hangkong University, China. His current research interests include robot application and welding robot.